LAWRENCE
LIVERMORE
NATIONAL
LABORATORY

LLNL-TR-400070

0.351 micron Laser Beam propagation in High-temperature Plasmas

D. Froula, L. Divol, N. Meezan, J. Ross, R. L. Berger, P. Michel, S. Dixit, V. Rekow, C. Sorce, J. D. Moody, P. Neumayer, B Pollock, R. Wallace, L. Suter, S. H. Glenzer

December 21, 2007

Disclaimer

This document was prepared as an account of work sponsored by an agency of the United States government. Neither the United States government nor Lawrence Livermore National Security, LLC, nor any of their employees makes any warranty, expressed or implied, or assumes any legal liability or responsibility for the accuracy, completeness, or usefulness of any information, apparatus, product, or process disclosed, or represents that its use would not infringe privately owned rights. Reference herein to any specific commercial product, process, or service by trade name, trademark, manufacturer, or otherwise does not necessarily constitute or imply its endorsement, recommendation, or favoring by the United States government or Lawrence Livermore National Security, LLC. The views and opinions of authors expressed herein do not necessarily state or reflect those of the United States government or Lawrence Livermore National Security, LLC, and shall not be used for advertising or product endorsement purposes.

This work performed under the auspices of the U.S. Department of Energy by Lawrence Livermore National Laboratory under Contract DE-AC52-07NA27344.

FY07 LDRD Final Report
0.351 micron LASER BEAM PROPAGATION IN HIGH-TEMPERATURE PLASMAS
Project Tracking Code: 06-ERD-056

Dustin H. Froula, Principal Investigator
(Dated: December 10, 2007)

A study of the laser-plasma interaction processes have been performed in plasmas that are created to emulate the plasma conditions in indirect drive inertial confinement fusion targets. The plasma emulator is produced in a gas-filled hohlraum; a blue 351-nm laser beam propagates along the axis of the hohlraum interacting with a high-temperature ($T_e = 3.5$ keV), dense ($n_e = 5 \times 10^{20}$cm^{-3}), long-scale length ($L \sim 2$ mm) plasma. Experiments at these conditions have demonstrated that the interaction beam produces less than 1% total backscatter resulting in transmission greater than 90% for laser intensities less than $I < 2 \times 10^{15}$ W-cm^{-2}. The bulk plasma conditions have been independently characterized using Thomson scattering where the peak electron temperatures are shown to scale with the hohlraum heater beam energy in the range from 2 keV to 3.5 keV. This feature has allowed us to determine the thresholds for both backscattering and filamentation instabilities; the former measured with absolutely calibrated full aperture backscatter and near backscatter diagnostics and the latter with a transmitted beam diagnostics. A plasma length scaling is also investigated extending our measurements to 4-mm long high-temperature plasmas. At intensities $I < 5 \times 10^{14}$ W-cm^{-2}, greater than 80% of the energy in the laser is transmitted through a 5-mm long, high-temperature ($T_e > 2.5$ keV) high-density ($n_e = 5 \times 10^{20}$ W-cm^{-3}) plasma. Comparing the experimental results with detailed gain calculations for the onset of significant laser scattering processes shows a stimulated Brillouin scattering threshold (R=10%) for a linear gain of 15; these high temperature, low density experiments produce plasma conditions comparable to those along the outer beams in ignition hohlraum designs. By increasing the gas fill density ($n_e = 10^{21}$cm^{-3}) in these targets, the inner beam ignition hohlraum conditions are accessed. In this case, stimulated Raman scattering dominates the backscattering processes and we show that scattering is small for gains less than 20 which can be achieved through proper choice of the laser beam intensity. The first three-dimensional (3D) simulations of a high power $0.351\mu m$ laser beam propagating through a high-temperature hohlraum plasma are also reported. We show that 3D linear kinetic modeling of Stimulated Brillouin scattering reproduces quantitatively the experimental measurements, provided it is coupled to detailed hydrodynamics simulation and a realistic description of the laser beam from its millimeter-size envelop down to the micron scale speckles. These simulations accurately predict the strong reduction of SBS measured when polarization smoothing is used.

I. INTRODUCTION

Inertial confinement fusion (ICF) and high energy density physics experiments[1, 2] with mega-joule class lasers[3, 4] require intense and energetic laser beams to propagate through large-scale length plasmas and to deposit their energy in the target for efficient production of soft or hard x rays. Radiation cavities, called hohlraums, are employed to confine the radiation and to efficiently produce thermal soft x-ray emission. In present indirect drive inertial confinement fusion designs, a fusion capsule is placed in the center of a hohlraum and the soft x rays from the walls are absorbed in the capsule ablator to implode and ignite the deuterium-tritium plasma. These hohlraums employed in ICF research use a low-Z cryogenic gas fill to prevent fast wall plasma blow off, which may impose asymmetric capsule implosion conditions. Consequently, the laser beams have to initially propagate through up to 1 cm of dense low-Z plasma before they deposit their energy in the hohlraum wall.

The physics of ignition hohlraums includes radiation production and confinement, and the laser-plasma interaction processes that determine laser beam propagation, scattering and absorption. Generally, predictive modeling of the laser-plasma interaction processes[5, 6] requires detailed understanding of instabilities including laser backscattering by Stimulated Brillouin Scattering (SBS) and Stimulated Raman Scattering (SRS), laser beam deflection, beam filamentation, and self focusing [7]. Moreover, a generally applicable quantitative model will need to include the different hohlraum materials and the nonlinear evolution of the instabilities. The development and testing of such a capability is an ongoing research activity and is presently providing guidance on experiments that apply high laser intensities. However, for the design of ignition hohlraum targets at the National Ignition Facility (NIF)[1, 8] a strategy to choose laser intensities and beam smoothing to produce conditions for which the gain exponent[9] of

various laser-plasma instabilities are small so that efficient laser beam propagation and high x-ray production may be expected.

In the studies funded by this project, we have determined, through experiments at the Omega laser facility [10], the plasma conditions and the range of gain exponents for laser-plasma instabilities that result in low backscatter and limited filamentation as required for ignition hohlraum plasmas. For this purpose, we have developed new high-temperature hohlraum targets that reach electron temperatures of up to $T_e = 4$ keV[11] at a scale length of $1 - 5$ mm and electron densities of $n_e/n_{cr} = 0.06 - 0.12$. Here, $n_{cr} = 10^{22}$cm^{-3} is the critical density for 351-nm laser light. For this study, CH-gas fills have been chosen emulating the present plasma conditions in ignition hohlraum designs[12].

The bulk plasma conditions are well characterized with Thomson scattering[11, 13, 14] allowing us to determine the gain values for which laser backscattering and filamentation processes become important. A 4ω-probe laser[15, 16] has been focussed into the center of the hohlraum and the ion feature of the optically Thomson-scattered spectrum was temporally resolved with a streaked spectrometer. Thus, the electron temperature, T_e, and the ion temperature, T_i, have been both measured accurately and simultaneously. In the present studies we find $T_e/T_i \approx 5$ and T_e is determined by the hohlraum heater beam laser energy providing a temperature range of 2 keV$< T_e < 3.5$ keV. Since SBS and SRS gain values are sensitive to T_e as well as to T_e/T_i, Thomson scattering has allowed us to directly calculate the laser-plasma interaction instability gains for each shot.

The SBS reflectivity has been measured by the absolutely calibrated full aperture backscatter and near backscatter diagnostics at Omega. These measurements are complemented by the transmitted beam diagnostics[17] that measures the transmitted laser power, spectrum, and the near-field laser beam spot. This complete suite of diagnostics allows us to determine the beam energetics by completely accounting for the scattered and absorbed laser power[18]. Furthermore, the transmitted laser beam spot measurements detect beam spray due to filamentation and self-focussing effects[19].

Two conditions have been extensively studied that correspond to the plasma regimes encountered by the laser beams in the different cones in an ignition hohlraum. NIF has 4 cones each with quads of beams that irradiate the hohlraum at 23°, 30°, 44°, and 50° to the hohlraum axis. Since the 44°, and 50° beams both primarily encounter hot ($T_e > 3$ keV) and dense ($n_e/n_{cr} = 0.06$) plasmas conditions before irradiating the hohlraum walls they are referred to as outer beams. The 23°, 30° beams, on the other had, first propagate through similar conditions like the outer beams before they encounter denser ($n_e/n_{cr} \simeq 0.1 - 0.15$) moderately hot ($2.5 < T_e < 3.5$ keV) plasmas conditions. They are accordingly noted as inner beams.

For the outer beam emulator conditions, we find that SRS is negligible and the backscatter is dominated by SBS light. By increasing the electron temperature of the plasma from $T_e = 2$ keV to $T_e = 3.5$ keV we find, for laser beam intensities of $I = 2 \times 10^{15}$ W-cm^{-2}, that the SBS reflectivity drops to < 1 % corresponding to a gain of $G_{SBS} < 15$.

For inner beam emulator plasma conditions with higher densities of $n_e/n_{cr} = 0.12$, we generally find that SRS dominates the backscattering and SBS is small ($< 10\%$), but not negligible. The high electron densities occur in ignition hohlraums in close proximity to the fusion capsule where the inner beams interact with the ablator blow off plasma. Optimizing the fusion capsule performance by choosing a hydrodynamicly efficient ablator, for example beryllium compared to CH, will cause the electron density in this region of the hohlraum interior to be significantly larger than for the outer beams. Our experiments show that SRS can be controlled and reduced to small levels of < 5 % for laser beam intensities of $I \simeq 4 \times 10^{14}$ W-cm^{-2}. These results provide important guidance for future ignition experiments. It is planned to choose the inner laser beam spots so that the intensity will remain below this limit at the position in the hohlraum where the beam begin interacting with the high-density plasma.

We have further studied backscatter mitigation techniques like laser beam smoothing and plasma conditioning. Polarization smoothing was demonstrated to significantly reduce the stimulated Brillouin threshold while adding hydrogen to a plasma reduces the backscatter from 20% to the percent level. This is a demonstration that the laser backscattering processes can be strongly suppressed in multiple-ion species plasmas.

Section II presents the experimental setup where the high-temperature hohlraum targets, the heater and interaction laser beam configurations, the suite of diagnostics, and radiation-hydrodynamics simulation results are presented. The laser backscatter measurements for the outer and inner beam hohlraum plasma emulator experiments are presented in Sec. III. The paper concludes in Sec. IV. Section V acknowledges those that made this research possible and Sec. VI lists the publications that have resulted from this project.

II. EXPERIMENT

A. High Electron-Temperature Targets [Phys. of Plasmas 14, 055705 (2007)]

The experiments were performed with the Omega Laser Facility at the Laboratory for Laser Energetics [10]. The laser facility consists of 60 frequency tripled Nd:glass laser beams with approximately 500 J per beam of 351 nm (3ω)
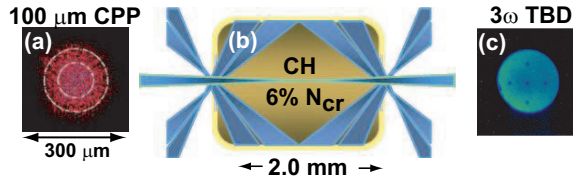
FIG. 1: (color) A 3ω interaction beam smoothed with a CPP (a) and a maximum power averaged intensity of $I_{100\mu m} < 4 \times 10^{15}$ W-cm^{-2} is aligned along the axis of a gas-filled hohlraum (b) where 33 heater beams heat the CH gas to a maximum electron temperature of 3.5 keV. The electron temperature at the center of the hohlraum is measured using Thomson scattering where the total heater beam energy has been scaled from 8 kJ to 17 kJ. The transmitted power and near field beam profile indicates a transparent plasmas for $T_e > 3$ keV.

laser light on target. In these experiments, one of the 3ω f/6.7 beams (B30) is fully equipped with laser backscattering and transmission diagnostics that has been configured as an interaction beam with dedicated Continuous Phase Plates (CPP) [20] , Smoothing by Spectral Dispersion (SSD), and appropriate delay with respect to the heater beams. A 2-mm long, 1.6-mm diameter gas-filled hohlraum has been aligned along the axis of the interaction beam so that the beam propagates through the heated hohlraum plasma (Fig. 1) interacting with a $\sim$ 2-mm long high temperature plasma. At the center of the hohlraum, laser beam intensities of up to $I \simeq 4 \times 10^{15}$ W-cm^{-2} have been achieved in the CPP-smoothed spot with a minimum vacuum diameter of 100 microns. The intensity of the interaction beam has been varied by changing the energy of the beam. A power average intensity of $I_{100\mu m} = E[J] \times 10^{13}$ W-cm^{-2}, where E is the incident laser beam energy ranging from 100 J to 400 J, is obtained using the $100\mu m$ phase plate. For intensities below $I < 1 \times 10^{15}$ W-cm^{-2}, a second 200 micron CPP is employed providing peak intensity of $I_{200\mu m} = 2.6 \times 10^{12}E[J]$ W-cm^{-2}.

The hohlraums are heated with up to 33 laser beams with total heater beam energy ranging from 8 kJ to 17 kJ in a 1 ns flat top laser pulse with 0.15 ns rising and falling edges. The heater beams penetrate the hohlraum at both ends through laser entrance holes with a diameter of 0.8 mm which are covered with 0.26 micron thick polyimide membranes to contain the gas fill. The choice of the initial hydro-carbon gas fill density allows us to vary the electron density in the interaction beam path for emulating outer or inner beam conditions.

The electron temperature along the interaction beam path is controlled by varying the heater beam energy from a maximum of 17 kJ; the plasma conditions along the interaction beam path have been measured using Thomson scattering. These measurements have validated 2-dimensional HYDRA [21] radiation-hydrodynamic simulations that show a uniform 1.6-mm plasma with a peak electron temperature of 3.5 keV [11]. The laser-plasma interaction experiments are performed in this well-characterized uniform hohlraum plasma at homogeneous density before shock waves driven by laser beam ablation at the gold wall reach the hohlraum axis, $t \simeq 1.3$ns (stagnation)[22].

The heat flux in the hydrodynamic modeling of the experiments is determined by either a flux limited diffusion model or a nonlocal model[23]. The primary difference between the nonlocal and flux limited models is the ability for the nonlocal model to inhibit the heat flux where there are large gradients while still allowing the fast electrons to carry away the heat. For example, in the presence of large temperature gradients, the flux limited model tends to either over estimate the heat flux (large flux limiter) artificially reducing the temperature gradient, or under estimate the heat flux (small flux limiter) therefore, preventing the surrounding plasma from getting hot. We find that both models indicate peak electron temperatures of order 3.5 keV in the 2 mm long flat density bulk plasma along the hohlraum axis. However, the nonlocal model shows larger temperature gradients resulting from the local laser beam heating that tends to reduce the calculated heat flux, therefore, increasing the temperature inside of the laser beams. The calculations indicate this heating around the laser entrance hole areas where several beams overlap. Such gradients have also been experimentally observed in previous Thomson-scattering measurements on the Nova laser facility [22]. However, the calculations of the bulk plasma conditions are insensitive to the choice of the heat transport modeling allowing linear gain calculations to correctly determine the gain for laser-plasma interaction processes in these targets.

This new target platform together with recently commissioned suite of laser-plasma interaction diagnostics [16, 17] allows the access to high temperature, long scale length conditions not previously available using gasbag [19, 24], toroidal hohlraum [25, 26], or gas-filled hohlraum targets. Laser-plasma interaction thresholds are sensitive to the electron temperature and the length of the density plateau in a plasma; electron temperatures in open geometry gasbag plasmas with roughly the same plasma scale-lengths are significantly lower than in the present hohlraum targets because of a factor of 10 larger energy density in hohlraums. Moreover, the capability to align the interaction beam along the hohlraum axis allowed us to reach significantly larger scale lengths than previous gas-filled hohlraum experiments[27] with the added benefits of accurate Thomson-scattering characterization and direct transmission measurements.
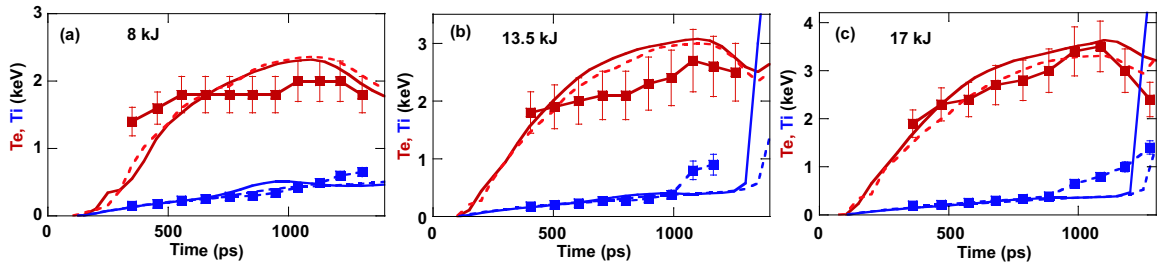
FIG. 2: (color) The electron (red) and ion (blue) temperatures from Thomson-scattering measurements at the center of the hohlraum is shown as function of time. The total heater beam energy has been varied (a) 8 kJ, (b) 13 kJ, (c) to 17 kJ indicating that the bulk plasmas conditions can be controlled. At the highest energies electron temperatures like those expected in ignition hohlraums are produced.

B. Thomson scattering [Phys. of Plasmas 13, 052704 (2006)]

The plasma conditions in the center of the hohlraum have been measured with 4ω Thomson scattering. One of the 3ω beams (beam 25) has been de-tuned to produce 2ω light and directed to a dedicated port (P9) and subsequently doubled to provide a 4ω Thomson-scattering probe laser [14, 16, 28]. Typical 4ω probe beam energies of E=200 J with a flat 1 ns pulse duration have been employed with a small focal spot of 60 μm at the Thomson-scattering volume. The scattered light is imaged, at a scattering angle of $\theta = 101^o$, through a diagnostic window (500 μm$\times$500 μm) cut in the side of the hohlraum wall. The hole is covered with a 0.26 micron thick polyimide window when a gas fill is employed. The scattering parameter is $\alpha = 1.4$ for plasma conditions of $T_e = 4$ keV and $n_e = 6 \times 10^{20}$ cm^{-3} where the scattering parameter α for our geometry is,

$$\alpha = 1 \times 10^{-10} \left(\frac{\mathrm{n}_e[\mathrm{cm}^{-3}]}{\mathrm{T}_e[\mathrm{keV}]} \right)^{1/2} \tag{1}$$

In our experiment $\mathrm{T}_i/\mathrm{ZT}_e$ is always smaller than the square of the scattering parameter ($\alpha^2 >\mathrm{T}_i/\mathrm{ZT}_e$), therefore, collective ion-acoustic modes are observed[29].

The wavelength shift of the ion-acoustic modes in the Thomson-scattering spectrum are determined by the plasma conditions (primarily temperature), probe laser wavelength, λ_0, and the scattering angle θ. Features are observed corresponding to ion-acoustic modes propagating and counter-propagating along the scattering vector $\mathbf{k}$ with $k = 4\pi/\lambda_0 \sin(\theta/2)$. For our conditions, the wavelength shift between the two ion acoustic peaks is of order $0.5 - 1$ nm[11].

To spectrally and temporally resolve the scattered light spectrum we fielded an achromatic collection system. The scattered light is collected and collimated by an $f/10$ achromatic lens with a 50 cm focal length. A blast shield with a coating to reject the scattered light from the 3ω heater beams has been implemented prior to the collection lens. A 7.5 cm focusing mirror with a 75 cm focal length images the scattered light onto the 150 μm slit of a 1-meter imaging spectrometer with a 3600 lines/mm grating. A high dynamic range streak camera is coupled to the spectrometer through a 200 μm temporal slit[14, 28].

The Thomson-scattering volume (60μm$\times110\mu$m$\times80\mu$m) is defined by the beam waist of the probe beam (60μm) and the projection of the spectrally and temporally resolving slits into the plasma. The location of the scattering volume is known to the accuracy of the target alignment system which is better than 50μm.

The scattered frequency spectrum provides a measure of the local particle flow velocity and the ion-acoustic sound speed that is directly related to the electron temperature. In our two-ion-species carbon-hydrogen plasmas, the relative amplitude of the light scattered from the two ion-acoustic modes allows an accurate determination of the ion temperature [30–33]. The results for the ion and electron temperatures at the center of the hohlraum are shown in Fig. 2 for 8 kJ, 13.5 kJ, and 17 kJ heater beam energy into the hohlraum [11].

C. Transmitted Beam Diagnostics [Rev. Sci. Instr., 77 10E507 (2006)]

The Transmitted Beam Diagnostics[17] measures the laser light transmitted through the target chamber center (TCC) within twice the original $f/6.7$ beam cone of the Omega Beam 30 operated at 3ω. At 60 cm past TCC, a 25-cm-diameter uncoated fused silica focusing mirror, $f = 44$ cm, directs 4% of the transmitted light through a 10-cm diameter port on the target chamber.

The beam propagates out of the target chamber onto a diagnostic table where the transmitted beam energy is directly measured using two calorimeters. One calorimeter measures the energy of the forward stimulated Brillouin scattering (FSBS) contribution and a second the forward stimulated Raman scattering (FSRS). In addition, a small fraction of the light is picked-off to measure the full-aperture transmitted power, spectrum, and a near-field image of the transmitted light. The FSBS and the FSRS measurement employ two spectrometers equipped with optical streak cameras.

While the total transmitted beam power is an important quantity to determine the energetics of the laser-plasmas interactions, the near field measurements provide the transmitted beam profile which directly measures beam spray induced by scattering processes and filamentation. The latter employs two gated intensified 16 bit CCD cameras imaging twice the initial $f/6.7$ cone with two 105 mm $f/4.5$ achromatic lenses. This system is capable to resolve beam spray of 1 degree.

D. Backscattering diagnostics

Light backscattered from the 3ω interaction beam is measured using a Full-Aperture Backscattering Station (FABS) and a Near Backscattering Imager (NBI). Light scattered back into the original beam f-cone is collected by FABS; both the SBS (350-352 nm) and the SRS (400-600 nm) spectrum and energy are independently measured. The FABS collects light that has been backscattered into the 30-cm focusing lens. The backscattered light is collimated by the lens and reflected by the last turning mirror. About 95% of the backscattered light is transmitted and picked off by a bare surface wedged optic.

The SRS and SBS light is separated by wedged optics and filters. Two calorimeters measure the total SBS and SRS energy. The system is calibrated *in situ* at 351 nm by the opposing laser beam at low-energy. Prior to the calorimeters a small fraction of the light is picked off into optical fibers and the SBS and SRS spectra are recorded using spectrometers equipped with optical streak cameras. The spectra were measured with a respective resolution of 0.5 nm and 0.05 nm.

The Near Backscatter Imager (NBI) measures the light outside of the original beam cone reflecting from a spectralon plate surrounding the interaction beam. The plate is imaged onto two charge-coupled devices (CCD) which time integrate the SBS and SRS signals. The cameras have been calibrated at 354 nm and 532 nm with a pulsed calibration laser of known energy that is reflected by the plate at various locations. These backscattering diagnostics (FABS and NBI) allow us to measure the total reflected light with an accuracy of ~ 20 %. By correlating the plasma parameters, backscatter, and transmission measurements we are able to obtain a detailed scaling of laser scattering as a function of electron density and temperature.

III. RESULTS AND DISCUSSION

A. Outer Beam Emulator [Phys. Rev. Lett. 98, 085001 (2007)]

Figure 3 shows a strong reduction in the backscattered light as the electron temperature along the hohlraum axis exceeds 3 keV [34]. The decrease in reflectivity with increasing temperature is a direct result of reducing the SBS three wave coupling as evident in the linear gain for intensity,

$$G_{sbs} = 290 \cdot \lambda_o[\mu m] \left(\frac{n_e}{n_{cr}} \right) \left(\frac{L[mm]}{T_e[keV]} \right) \left(\frac{\omega_a}{\nu_a} \right) I_{15}[\text{W-cm}^{-2}] \tag{2}$$

where $\frac{n_e}{n_{cr}} = 0.06$ is the fraction of electron density to the critical density for 3ω light and $L \sim 1.6$ mm is the plasma length. T_e/T_i changes by less than 15% and the Landau damping for our conditions is $\nu_a/\omega_a \approx 0.15$. The theoretical curve in Fig. 3 is obtained by applying linear theory including pump depletion [35],

$$R(1-R) = \epsilon e^{G_o \frac{T_o}{T_e}(1-R)} \tag{3}$$

where $\epsilon \approx 10^{-9}$ is the thermal noise. The peak linear SBS gain calculated by post processing the plasma properties from HYDRA simulations using the code LIP[9] is $G_o = 28$ for $T_o = 1.8$ keV. At this intensity ($I_{100\mu m} = 2 \times 10^{15}$ W-cm^{-2}) no backscattered light was detected by the NBI outside of the original beam cone. No SRS is measured in these experiments, as predicted by the moderate linear SRS gains ($G_{srs} < 20$).

The SBS spectra measured by FABS (Fig. 4a) shows a narrow feature that peaks when the interaction beam reaches maximum power and the plasma is cold ($T_e = 1.8$ keV). The temporal reflectivity and wavelength shift of
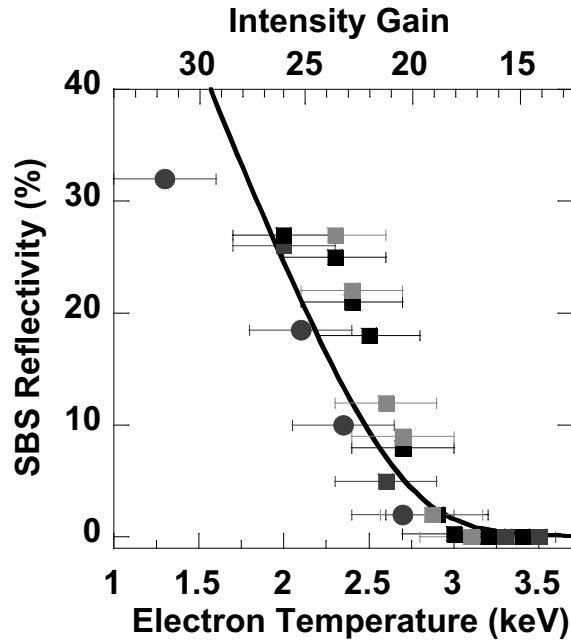
FIG. 3: The measured SBS reflectivity is compared directly to the electron temperature by temporally correlating the measurements for an interaction beam intensity of $I_{100~\mu m} = 1.7 \times 10^{15}$ W cm^{-2}. Each point represents an average over 200 ps and each shade of gray corresponds to a separate shot; the total heater beam energy is varied from 8 kJ (circles) to 16 kJ (squares). The reflectivity is calculated using Eq. 3 (solid curve). The linear gain (top axis) is calculated using Eq. 5. As the electron temperature reaches 3 keV, the SBS backscatter drops below detection levels ($< 1\%$).
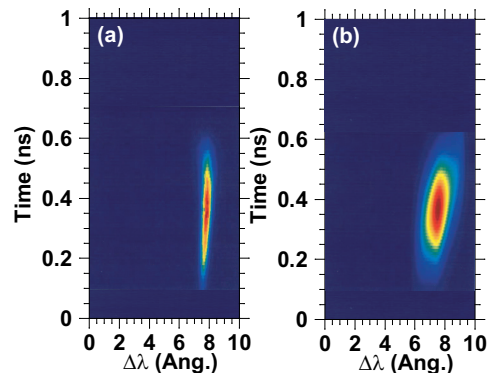
FIG. 4: (color) (a) The measured time-resolved SBS spectra for an intensity of $I_{100\mu m} = 2 \times 10^{15}$ W-cm^{-2} and 15.5 kJ of heater beam energy is shown. (b) A synthetic SBS spectrum is obtained by post-processing detailed hydrodynamic simulations with LIP and Eq. 3. The good agreement between these spectra confirms that SBS comes from the central density plateau. The wavelength shift ($\Delta\lambda = 7.5$Å) is consistent with the simulated electron temperature ($T_e = 1.8$ keV) during the first 200 ps of the experiment.

this spectra are well reproduced by the linear gain calculations shown in Fig. 4b where the SBS power spectrum has been calculated using linear theory, Eq. 3. The simulated reflectivity is consistent with the measurements when the instrument function ($\sigma = 100$ ps) has been convolved to account for the time smear introduced by the spectrometer[36]. Both the simulation and the experimental results show that when the plasma reaches a temperature above 3 keV, the total backscatter is less than 1%.

Furthermore, the simulated SBS frequency shift is consistent with the measured spectrum when correcting for the frequency change observed in the forward scattered light [9]. Figure 5 shows the wavelength of the light observed by the 3ωTBD blue-shifted by a few angstroms over the time of the experiment. This is attributed to the plasma density through which the light is propagating increasing in time [37]. The SBS reflected light also experiences this frequency upshift. Therefore to compare the measured spectra to the simulated spectra shown in Fig. 4, we add the magnitude
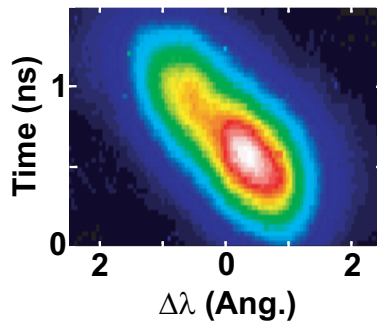
FIG. 5: The measured transmitted light spectra is blue-shifted due to the plasma density through which the light is propagating is increasing in time.
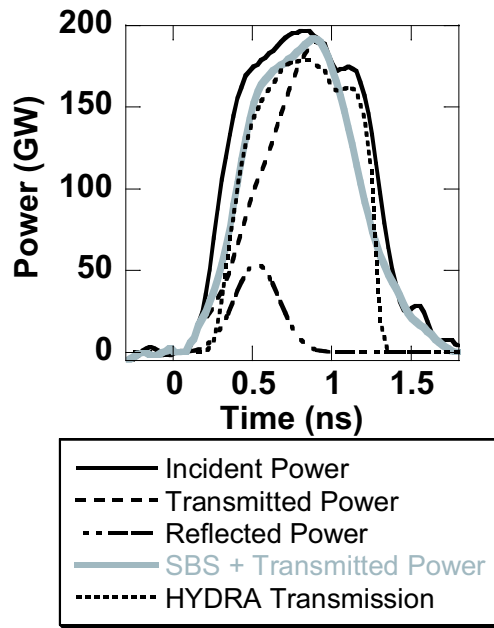

FIG. 6: The time-resolved measured (dashed) and calculated (dots) transmitted power is shown for conditions similar to those of Fig. 4. As HYDRA does not include backscatter, we add the measured SBS power (dot-dash) to the measured transmitted power (dashed) and obtain the solid gray curve which compares well. At peak electron temperature (t=900 ps), we measure a peak transmission above 90%.

of the wavelength shift measured in the transmitted light to the calculated spectra.

Low backscatter and high electron temperature leads to a peak transmission (Fig. 6) greater than 90% for intensities $I \leq 2 \times 10^{15}$ W-cm^{-2}. The total scattered power (3ωTBD + backscatter) compares well with HYDRA simulations that do not include backscatter losses but account for inverse bremsstrahlung absorbtion. The agreement between the measurements and calculations further indicates the lack of side scattering losses.

In addition to this high transmission, Fig. 7a shows that the transmitted beam remains in the original beam cone after propagation through the nearly 2-mm plasma. When the laser intensity is increased to $I = 4 \times 10^{15}$ W-cm^{-2}, Fig. 7b shows energy outside of the original beam cone.

Beam spray is a direct measure of filamentation; the filamentation threshold for an ideal beam can be calculated by balancing the plasma pressure with the pondermotive force resulting from the transverse profile of the laser beam [38]. Theoretical work using the laser-plasma interaction code Pf3D has extended this work to include the laser beam intensity profile with a continuous phase plate [39],

$$\frac{\lambda_o^2 I_{100\mu m}}{10^{13}} \left(\frac{n_e}{n_{cr}} \right) \left(\frac{3}{T_e} \right) \left(\frac{f^{\#}}{8} \right)^2 > 1 \tag{4}$$

where $I_{100\mu m} = E[J] \times 10^{13}$ W-cm^{-2} is the power averaged intensity at best focus, λ_o is the wavelength of the laser
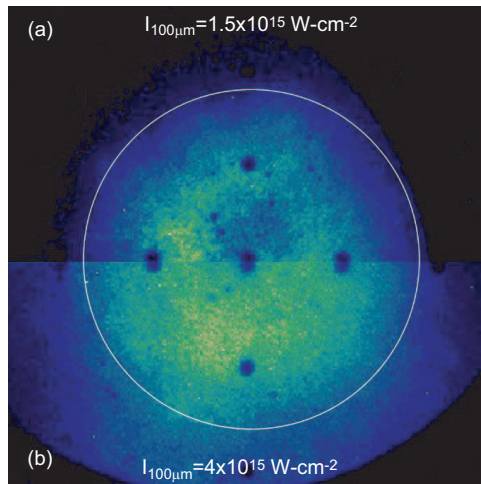
FIG. 7: The measured time integrated transmitted beam profiles are a shown for intensities of (a) $I_{100\mu m} = 1.5 \times 10^{15}$W-cm^{-2} and (b) $I_{100\mu m} = 4 \times 10^{15}$W-cm^{-2}; energy is measured outside of the beam cone for the highest intensity. Beam spray is a direct indication of filamentation in the plasma.
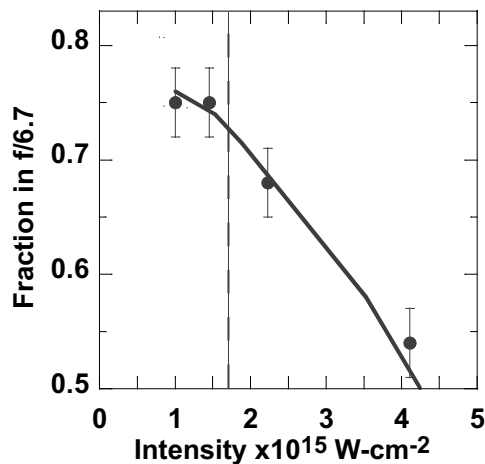

FIG. 8: For intensities less than $I_{FFOM} = 1.7 \times 10^{15}$W-cm^{-2}, 70% of the energy is measured to remain in the original $f/6.7$ beam cone.

beam, $n_e/n_{cr} = 0.06$ is the fraction of electron density to the critical density at 3ω, $T_e = 3.5$ keV is the electron temperature, and $f^\# = 6.7$ is the ratio of the focal length to the beam diameter. When the filamentation figure of merit (FFOM) is greater than one, the beam is expected to experience filamentation and beam spray.

Figure 8 shows that for an intensity less than I $< 2.0 \times 10^{15}$ W-cm^{-2}, 75% of the total transmitted power is measured within the original ($f/6.7$) beam cone. For intensities above this threshold, peak transmission drops to 70% and greater than 35% of the energy is outside of the original beam cone. Furthermore, backscattered light outside of the FABS is measured by the NBI. For the highest intensity shots ($I_{100\mu m} = 4 \times 10^{15}$ W-cm^{-2}), 50% of the total backscattered energy is outside of the original beam cone.

Our measurements presented in Fig. 8 are compared with the peak FFOM determined by post-processing the parameters calculated by the hydrodynamic simulations where the filamentation threshold is calculated to be at $I_{FFOM} = 1.7 \times 10^{15}$ W-cm^{-2}; at intensities less than this threshold, there is good laser beam propagation through the plasma.
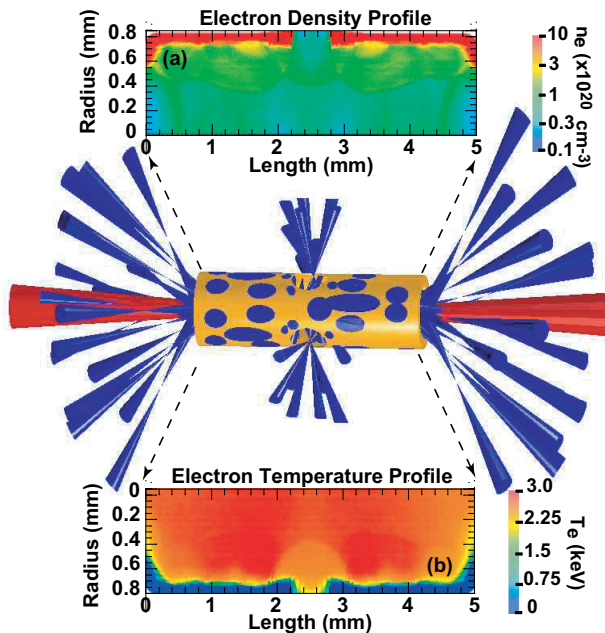
FIG. 9: The simulated (a) electron density and (b) electron temperature profiles are shown for the 5-mm long hohlraum at peak electron temperature (900 ps after the heater beams turn on). Three LEHs are equally spaced around the hohlraum equator to allow the addition of 17 laser beams. In total, fifty 3ω laser beams irradiate the hohlraum wall, producing electron temperature along the axis in excess of $T_e > 2.5$ keV. The interaction beam is aligned along the axis of the hohlraum interacting with a uniform 5×10^{20} cm^{-3} plasma plateau.

B. Inner Beam Plasma Emulator Results

1. Laser-Entrance Hole Region [Phys. Rev. Lett. Accepted (2008)]

In the indirect drive approach to inertial confinement fusion (ICF), laser beams will propagate through centimeter-scale under-dense ($n_e \simeq 5 \times 10^{20}$ cm^{-3}) plasmas prior to producing soft x-ray radiation near the inner wall of the radiation cavity (hohlraum) [8, 40]. Scaling the plasma length beyond 2 mm challenges both the current state-of-the-art laser-plasma interaction modeling and experimental facilities through computational requirements to resolve micron scales over many cubic millimeters of plasma and laser power to heat the large (L=5 mm) plasmas to relevant temperatures ($T_e > 2.5$ keV).

In this study, we demonstrate that backscatter in a 4-mm long plasma at electron temperatures above 2.5 keV can be controlled at ignition plasma conditions and intensities. These results span the gap between previous studies ($L < 2$ mm, $T_e \simeq 2.5$ keV) and future ignition hohlraum plasmas ($L \simeq 5$ mm, $T_e > 3$ keV). The experiments show that for an intensity of $I_{200\mu m} = 6 \times 10^{14}$ W-cm^{-2} the backscatter increases from $< 0.05\%$ to $> 10\%$ when increasing the length of the plasma from 1.3 mm to 4.0 mm. The intensity threshold, defined at the point when 5% of the incident power is backscattered, is measured to be $I_{5mm} = 4 \times 10^{14}$ W-cm^{-2} for propagation through this 5-mm long target while the threshold is a factor of 2.5 higher in the 2-mm long target ($I_{2mm} = 10 \times 10^{14}$ W-cm^{-2}). Increasing the intensity significantly above these thresholds, results in saturation due to pump depletion. These results have tested an exponential scaling model used to predict scattering from large scale-length ignition plasmas. Furthermore, the results compare well with a new laser-plasma interaction code (SLIP) [41] designed to simulate long 3D plasmas with large diameter laser beams encountered in the future ignition experiments.

For this study, new hohlraum targets have been designed for investigating laser-plasma interactions in 2-mm, 3.5-mm, and 5-mm long high-temperature plasmas (Fig. 9). The three gold hohlraums have the same diameter (1.6 mm) and produce a uniform density plateau using a room temperature 1 atm gas fill consisting of 30% CH$_4$ and 70% C$_3$H$_8$ expressed as partial pressures. To maintain high temperatures as the hohlraum is lengthened, the laser heater beam power must be increased. The hydrodynamic simulations exhibit a large region of gas and blow-off plasma inside the hohlraum that is nearly isothermal. The temperature of the isothermal region is controlled by a balance of laser heating with increasing thermal energy, radiation cooling, and electron heat transfer to the cold gold walls. The energy loss scales approximately linearly with the hohlraum length, since the loss to the LEHs and to the hohlraum end caps
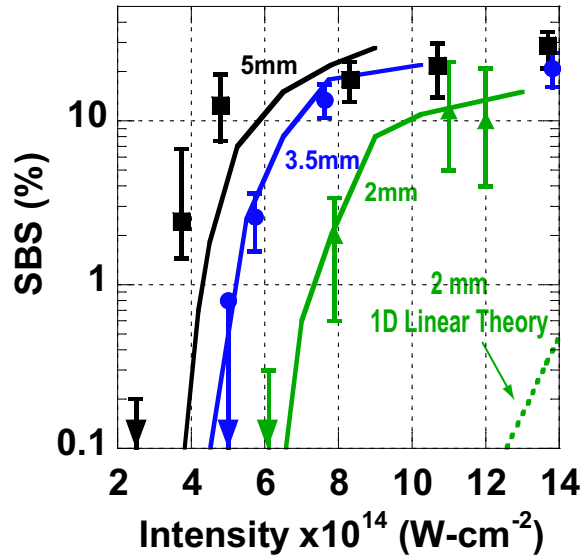
FIG. 10: (color) The measured instantaneous SBS reflectivity is plotted as a function of vacuum intensity for the three target lengths: 2 mm (triangles), 3.5 mm (circles), and 5 mm (squares). The solid curves are simulations performed by SLIP. For reference, a curve is shown (dashed) calculated using linear theory for the 2-mm long targets where a gain of $G_{sbs} = 11$, for an intensity of 1×10^{15} W-cm^{-2}, is determined by post processing the hydrodynamic parameters.

is fairly small. Therefore, maintaining a constant laser power per unit length keeps the temperature approximately constant as the length is increased. The addition of 17 heater beams that enter through the LEHs on the equator of the hohlraum allows us to keep the total laser power per unit length roughly constant between the 2-mm and 3.5-mm targets; this produces hot $T_e > 2.5$ keV plasmas for all three targets platforms.

Figure 10 demonstrates a plasma-length scaling for various interaction beam intensities. Extending the plasma length from 1.3 mm to 4.0 mm reduces the intensity threshold from $I_{2mm} = 10 \times 10^{14}$ W-cm^{-2} to $I_{5mm} = 4 \times 10^{14}$ W-cm^{-2} as predicted by the linear scaling of the gain exponent. As a result, the measured reflectivity shows an exponential growth from $< 0.05\%$ to $> 10\%$ when the plasma length increases from $L_{2mm} = 1.3$ mm to $L_{5mm} = 4$ mm at an intensity of $I_{200\mu m} = 6 \times 10^{14}$ W-cm^{-2}. The interaction beam intensity is known to better than 10%. The data points in Fig. 10 are obtained at a time 700 ps after the rise of the heater beams and averaged over 50 ps. The error bars are given by the upper and lower limits within this average. No SRS ($R_{srs} < 1\%$) is measured in these experiments while the heater beams are on (up to 1.1 ns), as expected by the moderate linear SRS gains ($G_{srs} < 10$) [9].

The simulated SBS reflectivities shown in Fig. 10 are in good agreement with the measurements. They were calculated by a recently implemented steady state paraxial coupled-wave-solver (SLIP). SLIP solves the linear kinetic model for SBS using the complete 3-dimensional plasma parameters, the measured near field of the interaction beam, and near-field phase induced by the CPP. The ability of SLIP to include the 3-dimensional nature of the spatially smoothed laser beam is a significant improvement over the standard 1D linear gain calculations (LIP) that are limited to geometric ray propagation [42]. This is evident in Fig. 10, where the linear gain calculations significantly underestimate the backscatter. Near the threshold, SLIP calculates the most intense speckles within the laser focal spot to trigger SBS locally while the average intensity used in LIP is still under the threshold. Even when the backscatter from these high intensity speckles remain small, they can act as increased noise source and trigger SBS for the whole beam, making the 1D model inaccurate.

2. Capsule Blow-Off Region

Laser-plasma interaction experiments in hohlraums filled with higher gas densities have been performed at Omega to emulate the plasma conditions encountered by the inner laser beam when they approach the dense capsule blow-off plasma in an ignition hohlraum. These experiments employ fill gas densities yielding electron densities of $n_e/n_{cr} = 0.11$ and electron temperatures of $T_e \approx 3$ keV at a scale length of 1.6 mm. These conditions are particularly relevant for 1.8 MJ ignition designs while, on the other hand, recent ignition hohlraum calculations for 1 MJ laser energy indicate even higher densities (up to $n_e/n_{cr} = 0.15$) and lower temperatures ($T_e = 2.5$ keV) in a shorter part of the laser beam
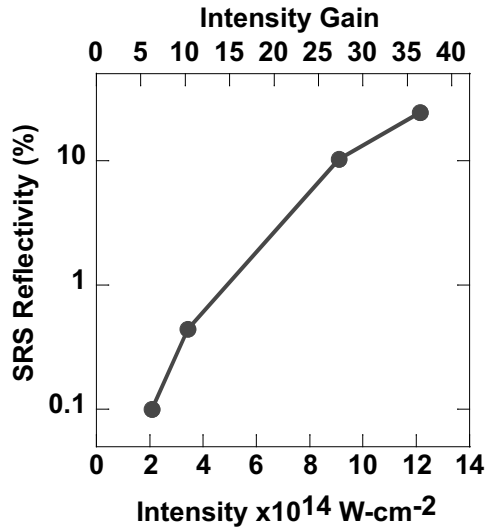
FIG. 11: The SRS reflectivity is shown to increase with the interaction beam intensity. For these conditions ($n_e/n_{cr} = 0.11$), an intensity threshold is measured at $I_{200\mu m} = 7 \times 10^{14}$ W-cm^{-2}.

path of $\sim 500\mu$m. Presently, these shorter scale length conditions have not been investigated at Omega and will be the focus of future work.

At high electron densities, we find that SRS is the dominant backscatter process. Figure 11 shows a strong dependency of the SRS backscattered light on the interaction beam intensity. The SRS reflectivity is reduced from $> 10\%$ to $< 1\%$ when reducing the intensity from $I_{200\mu m} = 1.2 \times 10^{15}$ W-cm^{-2} to $I_{200\mu m} = 2 \times 10^{14}$ W-cm^{-2}. In particular, for $I_{200\mu m} < 5 \times 10^{14}$ W-cm^{-2} we find that SRS is negligible, $< 1\%$ while SBS is $< 5\%$. As it was found for SBS, this decrease of the SRS reflectivity with decreasing intensity can be explained by a reduction of the SRS three wave coupling as evident in the linear gain. We find that gain values < 25 are required to obtain small scattering losses in these conditions. Besides accessing higher density shorter scale conditions, future work is intended to provide a better estimate of the maximum possible gain in this regime by performing experiments with intensities of $I = (6 - 8) \times 10^{14}$ W-cm^{-2}. These data will be important because present designs of the inner beam focal spot indicate intensities in this regime.

C.   Laser-Plasma Instability Mitigation Techniques

1.   Laser beam smoothing in ignition plasmas [Phys. Rev. Lett. submitted 2007]

To shape the laser focal spot and to smooth the inherent abberations produced by large high power glass lasers, continuous phase plates (CPP) [20] are used. These CPPs create a high contrast intensity pattern in the target plane with small-scale high-intensity structures (speckles). These speckles can play an important role in the dynamics of the laser-plasma interactions [43–47]. The high intensity contrast created by the CPP can instantaneously be reduced when applying polarization smoothing to the laser beam [48, 49].

Experiments in long-scale plasmas have shown the effect of polarization smoothing on the reduction of filamentation [50] and have demonstrated small reductions in backscatter [24, 51–53]. These experiments were performed at intensities well above the threshold for backscatter and the main effect of polarization smoothing on the backscatter was inferred to be through the mitigation of ponderomotive filamentation. The effect of polarization smoothing was further investigated at lower electron temperatures ($T_e < 1$ keV) and in short scale-length plasmas where it was shown that polarization smoothing indeed strongly reduces thermal filamentation in speckles leading to a reduction in backscatter [54–56].

In this study, we present experiments that demonstrate, the significant reduction of stimulated Brillouin scattering by polarization smoothing in conditions with no filamentation. We present measurements that show adding polarization smoothing increases the intensity threshold for SBS by a factor of 1.7 ± 0.2. For intensities less than 2×10^{15} W-cm^{-2}, more than an order of magnitude reduction in the backscattered power is observed. The study is performed in our high temperature ($T_e \simeq 3$ keV) ICF relevant plasma where ponderomotive and thermal filamentation effects are measured to be negligible.
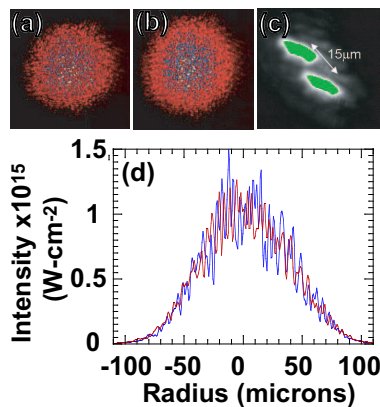
FIG. 12: (color) The far-field intensity distribution is simulated using the Omega laser beam abberations, the (a) measured CPP phase, and the (b) measured PS shift. (c) The polarization shift at the best vacuum focus was measured to be 15 microns. (d) The vacuum transverse intensity profile is compared with (red) and without polarization smoothing (blue) demonstrating an undetectable change in the average intensity when polarization smoothing is applied.

Figure 12a shows the simulated far-field laser spot for the 3ω interaction beam focused by a $f/6.7$ lens through a CPP. The simulated spot is generated using the Omega abberation model and the measured CPP near field phase. Figure 12d shows the intensity profile of the simulated laser spot averaged over 50 microns. The average on axis intensity at best focus for this beam is $I_{100\mu m} = 1.05 \times \text{P[GW]} \times 10^{13}$ W-cm^{-2}, where P is the incident laser beam power ranging from 50 GW to 500 GW.

A new birefringent polarization smoothing crystal has been designed for these experiments that sufficiently separates the speckles in the far field without affecting the average spot size. After the laser beam propagates through this crystal, two beams separated by a small angle are created with equal intensity and orthogonal polarizations. The separation between the two beams was characterized to be 15 microns at best vacuum focus (Fig. 12c). When used with a CPP, this 15 micron separation at the focal plane is sufficient to decorrelate the two speckle patterns while having a minimal effect on the average intensity of the laser beam (Fig. 12d).

Figure 13 shows that the intensity threshold for a CPP smoothed laser beam is $I_{th} = 1.3 \times 10^{15}$ W-cm^{-2}. Adding polarization smoothing increases this threshold to $I_{th} = 2.2 \times 10^{15}$ W-cm^{-2}. This factor of 1.7 ± 0.2 increase in the experimentally determined SBS threshold is consistent with modeling. Furthermore, polarization smoothing reduces the SBS reflected power by more than a factor of 10 for an incident intensity below $I = 2 \times 10^{15}$ W-cm^{-2} and about a factor of 3 for incident intensities between 2×10^{15} W-cm$^{-2} < I < 5 \times 10^{15}$ W-cm^{-2}, where the latter condition approaches the heavily driven regime where pump depletion becomes a factor. Adding 3Å of SSD to the bandwidth of the interaction beam has no measurable effect on SBS (Fig. 13). The SBS power is obtained by averaging the temporally resolved SBS reflectivity over 50 ps, 700 ps after the rise of the heater beam, prior to the shock wave produced by the ablation of the gold wall reaching the hohlraum axis, around t $\simeq$ 1.1ns. The error bars are given by the extreme reflectivities within the 50 ps time interval.

This measured enhancement of the SBS threshold is explained by a simple model that quantifies the effects of beam smoothing on the growth of SBS. In this model, we divide the plasma in to $n = L/L_{sp} = 19$ one-speckle-long slabs ($L_{sp} = 5f^2\lambda = 78$ μm). By averaging the SBS growth over the intensity distribution for a laser beam model with a CPP, $P(I) = \exp(-I)$, the average gain exponent over one slab is $\langle G_{sp}^{CPP} \rangle \simeq G_{sp}(1 + G_{sp}/2)$ provided the linear gain over one speckle is small ($G_{sp} \equiv G_{1D}/n << 1$) [44]. The gain over the entire plasma length (L=1.5 mm) is then given by adding the gain from each independent slab,

$$\langle G^{CPP} \rangle \simeq n\langle G_{sp}^{CPP} \rangle \simeq G_{1d}\left(1 + \frac{G_{sp}}{2}\right) \tag{5}$$

From here it is evident that the effective gain is increased from the 1D value when the intensity distribution created by the CPP is included. At the measured threshold intensity ($I_{th}^{CPP} = 1.3 \times 10^{15}$ W-cm^{-2}), the 1D gain is $G_{1D} = 14.4$. This leads to a gain per speckle of $G_{sp} = 0.7$ and a correction to the 1D gain of $\langle G \rangle/G_{1d} = 1.4$. Using Eq. 5, the scattered reflectivity can be calculated by exponentiating the linear gain $[R \sim \epsilon \exp \langle G \rangle]$ from an effective thermal noise determined by fitting the DEPLETE noise source calculations ($\epsilon = 10^{-11}$). The result agrees well with the experimental measurements (Fig. 13).

This model can be extended to include the effects of polarization smoothing. By splitting the power into two independent speckle patterns with orthogonal polarizations, the intensity distribution becomes $P(I) = 4I \exp(-2I)$.
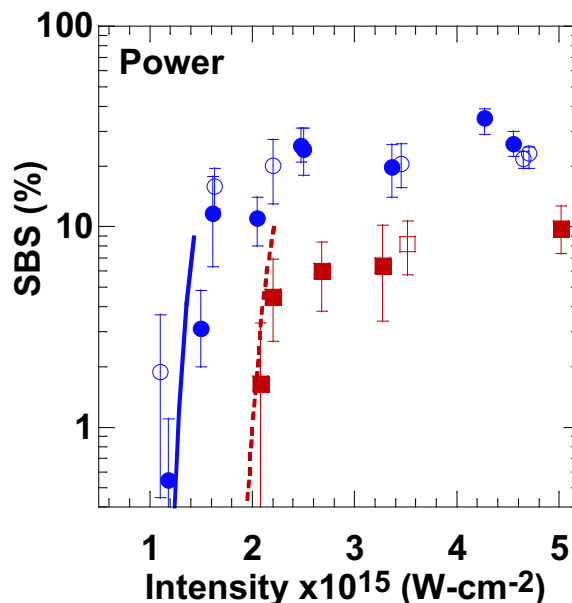
FIG. 13: (color) The measured instantaneous SBS reflectivity at 700 ps is plotted as a function of the interaction beam intensity; three laser smoothing conditions are shown: CPP (blue), PS (red), and 3Å SSD (open symbols). The calculated reflectivities using an analytical model reproduce the measured thresholds and the factor of 1.7 reduction in the SBS threshold when polarization smoothing is applied to a CCP smoothed laser beam. An analytical model (Eqs. 5 and 6) that calculates the thresholds is shown for the CPP only (solid blue curve) and when polarization smoothing is applied (dashed red curve).

Further assuming that the polarizations are uncorrelated between successive slaps of speckles, the average gain exponent over the entire plasma length is obtained,

$$\langle G^{ps} \rangle \simeq -n \ln \left(\frac{1}{2} - \frac{1}{(4 - 2G_{sp})^2} \right) \simeq \frac{G_{1d}}{2} \left(1 + \frac{G_{sp}}{2} \right) \tag{6}$$

This is a factor of 2 lower than Eq. 5, and the corresponding reflectivities agree well with the experiment (Fig. 13). Note that while the decrease in the SBS threshold over the 1D result is due to the high beam contrast when a CPP smoothing is applied, the increase when PS is applied results from the mixing of the polarizations, not to a reduction of the beam contrast. This effect of PS applies to any high-temperature, long plasma where the gain per speckle remains much less than two, as is the case for most of the current ignition designs for NIF.

2. Suppression of SBS using multiple-ion species plasmas [Phys. Rev. Lett. submitted 2007]

An important plasma parameter in controlling laser-plasma interactions is plasma-wave damping. At the high-electron temperature laser-heated plasma conditions, typical in ICF targets, ion-Landau damping in single-ion species plasmas is negligible. Landau damping due to electrons is small and of the order of 0.01, due to the large mass difference between electrons and ions. However, in multiple ion species plasmas, the number of charged particles close to the phase velocity of the SBS driven fast ion-acoustic mode is greatly enhanced effectively providing Landau damping.

A long-standing problem in the field of laser-plasma interactions is a successful demonstration that multiple ion species plasmas lead to reduced backscattering at ICF hohlraum conditions. Although the effect of two-ion species plasmas on Landau damping has been directly observed with Thomson scattering [11, 33], previous laser-plasma interaction experiments have not observed the expected reduction of SBS reflectivity with increased Landau damping. In addition, the experiments showed that SRS strongly increased reaching levels of more than 20% [?]. These experiments have been performed with a limited set of beam smoothing options or in low temperature plasmas where laser beam filamentation exceeds the growth threshold.

Here, we demonstrate that laser backscattering processes are strongly suppressed in multiple-ion species plasmas. Adding hydrogen to a hohlraum filled with CO2 is shown to reduce SBS reflected energy from 20% to the percent level. This is accompanied by a simultaneous increase of the transmitted energy of an axial interaction laser beam
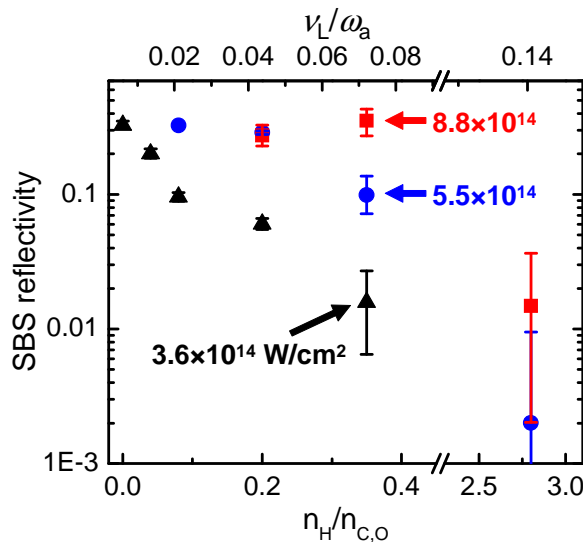
FIG. 14: (color) Instantaneous SBS reflectivities at t = 0.7 ns for interaction beam intensities of 3.6, 5.5 and 8.8×10^{14} W-cm^{-2}. Also shown are the Landau damping values increasing from 0.006 to 0.13.

and increased radiation temperature of the hohlraum. The measured scaling of SBS with increasing Landau damping agrees with linear gain calculations. Full scale 3D laser-plasma interaction simulations reproduce these findings and further indicate that SBS can be efficiently controlled by employing multiple-ion species plasmas on future ICF experiments on the NIF.

Figure 14 shows the instantaneous SBS reflectivity for varying the ratio of heavy to light ion species (r_H) at t = 0.7 ns. For the probe beam intensity of 3.6×10^{14} W-cm^{-2} the reflected power is gradually reduced from 30% to the percent level when increasing the hydrogen fraction to $r_H = 0.35$, i.e. when increasing Landau damping from $\nu_L/\omega_a = 0.006$ to $\nu_L/\omega_a = 0.025$. For higher probe beam intensities, the reflectivity is reduced if higher hydrogen fractions are employed, indicating strong saturation of the SBS instability, e.g., by pump depletion. The error bars are mainly due to the uncertainty in the relative timing of about 100 ps. We note that in all cases the level of SRS backscattered light was below the instrumental detection threshold, i.e. below $\sim 10^{-4}$.

D. Predictive 3D modeling of SBS in ignition-scale experiments [Phys. Rev. Lett. submitted (2007)]

One of the grand challenge of laser-plasma interaction (LPI) studies is to provide guidance for the design of hohlraum targets on the next generation of laser facilities for ignition attempts [3, 8]. Modeling LPI processes in real-size experiments has been recognized as a difficult task. One of the main difficulties is the vast parameter space in electron density, temperature and spatial scales that are typically spanned by an ignition relevant laser-plasma experiments on current laser facilities. This leads to a plethora of (usually coupled) LPI processes such as absorption, refraction, diffraction, filamentation and parametric backscattering instabilities [7]. Another challenge is the proper description of the spatially smoothed laser beams used on all modern facilities, which exhibit intensity structures from the hundreds of microns down to the micron scale [6].

In this study, we report on three dimensional simulations of a whole laser beam propagating through an ignition-scale experiment, using the fluid paraxial code pF3d. These simulations include models for both stimulated Raman (SRS) and Brillouin (SBS) backscattering. We show that a fluid-based modeling of SBS including linear kinetic correction, coupled to accurate hydrodynamics profiles and a realistic description of the laser intensity pattern generated by various smoothing smoothing options leads to quantitative agreement between the measured and calculated reflectivities over many order of magnitude and for different smoothing techniques (polarization smoothing and smoothing by spectral dispersion).

We are interested here in validating LPI modeling tools in conditions close to future ignition experiments. In this letter we model a series of recent experiments (see Sec. II).

A number of steps are necessary in order to confidently compare pF3d simulation results with the measured reflectivities. First we need accurate plasma parameters as input for pF3d. Extensive Thomson scattering measurements (see Sec. II B) in the multispecies plasma (C and H atoms) allowed to measure both the electron and ion temperatures at the center of the target, as well as the density evolution. These time-resolved measurements were successfully compared
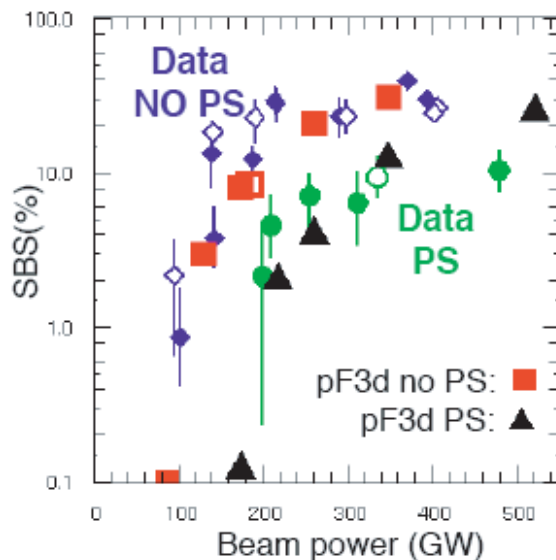
FIG. 15: (color) Measured (blue diamonds and green circles) and calculated (red squares and black triangles) SBS reflectivity as function of laser power at t=700 ps. Both the measurement and simulations show a factor of two increase in the SBS threshold when PS is used. Empty symbols corresponds to measurements and simulations with 3Å of SSD added. pF3d results quantitatively match the measured reflectivity over more than two order of magnitude for all smoothing techniques employed.

to HYDRA simulations and show relative insensitivity to the exact heat conduction model employed[meezan2007]. We can then directly use HYDRA three-dimensional hydrodynamics maps (electron density Ne and temperature Te, ion temperature Ti and plasma flow) as initial conditions for pF3d. We perform post-shot HYDRA simulations to account for variation in heater beam energy (typically $< 4\%$) and gas fill pressure ($< 10\%$) between shots.

Second, a realistic description of the laser beam is needed. We use the measured continuous phase plate (CPP) phase mask used on the interaction beam and a model for Omega beam aberrations. The simulation resolves both the envelop of the beam, which is close to a Gaussian with $100\mu m$ FWHM at best focus and the f/6.7 speckles at the micron scale. The typical resolution required by the paraxial approximation used for laser propagation is $dx = dy = 1.3\lambda_o m$ and $dz = 4\lambda_o$. The plasma volume modeled encompasses more than a billion cells. It is difficult to define an average laser intensity for such a beam, but a benefit of 3D whole beam simulations is that only the beam power (here in the 100-400 GW range) is needed as an input parameter. As a reference, the intensity averaged over a $50\mu m$ volume at best focus is 1.05×10^{15} W.cm^2 for an input power of 100 GW. Additional beam smoothing techniques are equally accurately modeled (see Sec. III C 1). When polarization smoothing (PS) [?] is used, pF3d solves paraxial equations for each polarization component, with the two speckle patterns being offset in the far field by the experimentally measured shift induced by the PS wedge. Smoothing by spectral dispersion (SSD) is modeled using the correct modulator, grating geometry and depth of modulation.

Third, a detailed fluid-based model has been developed to describe the response of the plasma to the ponderomotive drive and is described in [5]. Here we will focus on the details of the SBS model which was dominant in the experiment. Stimulated Raman backscatter was below measurement threshold for all powers and negligible in simulations too, as expected in low density, high temperature plasmas where Landau damping is large.

Figure 15 shows the measured and simulated SBS reflectivity as function of the interaction beam power. It is worth noting that our modeling does not allow for any free parameter: the laser and plasma parameters used as boundary and initial conditions are given by measurements or integrated simulations validated by measurements, while the SBS model is closed and derived from first principle linearized equations. The calculated Pf3D SBS reflectivities agree quantitatively with measurements over more than 2 order of magnitudes. pF3D predicts correctly the large increase in the SBS threshold when PS is used, as well as the absence of any measurable reduction of SBS when 3Å of SSD is added. The SBS signal simulated is almost entirely contained in the beam f-cone, which is consistent with the experiment.

Turning off the filamentation instability in a few simulations reduced the reflectivity near threshold, but the overall result was very close to Fig. 15. This is consistent with the high electron temperature and moderate laser intensity, which results in weak self-focusing of speckles and limited change to the beam contrast. Thus, the factor of 2 increase in the SBS threshold when PS is used is not due to a control of the filamentation instability [50] but to a direct mitigation of the SBS growth.

Indeed, the average laser intensity does not exceed the so-called critical intensity for SBS (corresponding to an e-fold amplification over one speckle length) until very large reflectivities are observed. In this regime of low amplification over any speckle, a single row of speckles can act as an enhanced noise source but has a negligible contribution in the overall reflectivity, which is determined by amplification over many successive rows. When PS is used, on average only one or the other polarization is amplified over any speckle, which leads in the limit of small amplification per speckle, to a reduction of 2 of the overall gain exponent throughout the whole plasma (See Eqn. 6). This is observed both in the experiment and in the simulations (Fig. 15).

While developing a general predictive modeling capability for LPI remains a challenge, we have made a significant step towards that goal by using a detailed description of the plasma conditions and the laser beam intensity pattern as input to full 3D fluid-based LPI simulations done with our massively parallel code pF3d. This experimental validation is for now limited to stimulated Brillouin backscatter in a regime where kinetic and fluid nonlinearities are not expected to play a significant role (long hot plasma at moderate density and laser intensity). This is a regime of interest for forthcoming attempts at ignition on NIF and LMJ.

IV. SUMMARY AND OUTLOOK

In summary, we have demonstrated laser beam propagation through ICF hohlraums at ignition plasma conditions. This is accomplished through high electron temperature plasmas that reduce the linear gains below their thresholds ($G_{SBS,SRS} < 20$, FFOM< 1). For outer ignition laser beam conditions, where the electron temperatures are above 3 keV, the total backscatter is shown to be below 1% while producing a transparent plasma with a peak transmission greater than 90%. The laser beam is shown to propagate without beam spray for intensities below 2×10^{15} W-cm^{-2}; above this intensity the beam is shown to filament.

For inner ignition hohlraum laser beam conditions, the relevant laser beam intensities are smaller than for outer beam conditions, electron densities are larger and temperatures are smaller resulting in scattering levels that are increased for a given laser beam intensity. For present ignition designs, the intensity remains below $< 8 \times 10^{14}$ W-cm^{-2}. This is accomplished by choosing the appropriate laser spot and through absorption before the beam interacts with the higher density capsule blow-off plasma. In these conditions, the present experiments indicate that scattering levels < 5% may be achieved.

While developing a general predictive modeling capability for LPI remains a challenge, we have made a significant step towards that goal by using a detailed description of the plasma conditions and the laser beam intensity pattern as input to full 3D fluid-based LPI simulations done with our massively parallel code pF3d. This experimental validation is for now limited to stimulated Brillouin backscatter in a regime where kinetic and fluid nonlinearities are not expected to play a significant role (long hot plasma at moderate density and laser intensity). This is a regime of interest for forthcoming attempts at ignition on NIF and LMJ.

The present experiments verify the ability of current models to predict ignition hohlraum conditions and laser-plasma interaction linear gains for filamentation, SBS, and SRS. Furthermore, these results show the importance of predicting the electron temperature prior to peak power when the plasma is cold and the linear gains are near the backscatter thresholds; a small change in the electron temperature can lead to a significant increase in the backscattered energy. These issues will be addressed in future experiments where we plan to continue scattering measurements in high-electron temperature targets under a wide range of densities, materials, and laser smoothing conditions.

V. ACKNOWLEDGMENTS

VI. PUBLICATIONS RESULTING FROM THIS PROJECT

1. Pushing the limits of plasma length in inertial fusion laser-plasma interaction studies, D. H. Froula, L. Divol, R. London, D. Berger, N. B. Meezan, P. Neumayer, J. S. Ross, R. Wallace, and S. H. Glenzer, Accepted to Phys. Rev. Lett. (2008)

2. Predictive three dimensional modeling of Stimulated Brillouin Scattering in ignition-scale experiments, L. Divol, R. L. Berger, N. B. Meezan, D. H. Froula, S. Dixit, L. J. Suter and S. H. Glenzer, Submitted to Phys. Rev. Lett. (2007)

3. Suppression of Stimulated Brillouin Scattering by Increased Landau Damping in Multiple-Ion Species Hohlraum Plasmas, P. Neumayer, R. L. Berger, L. Divol, D. H. Froula, R. A. London, B. J. MacGowan, N. B. Meezan, J. S. Ross, C. Sorce, L. J. Suter, and S. H. Glenzer, Submitted to Phys. Rev. Lett. (2007)

4. Direct measurements of an increased threshold for stimulated Brillouin scattering with polarization smoothing in ignition hohlraum plasmas, D. H. Froula, L. Divol, R. L. Berger, R. A. London, N. B. Meezan, D. J. Strozzi, P. Neumayer, J. S. Ross, S. Stagnito, L. J. Suter, and S. H. Glenzer, Submitted to Phys. Rev. Lett. (2007)

5. Ideal laser beam propagation through high temperature ignition hohlraum plasmas, D. H. Froula, L. Divol, N. Meezan, S. Dixit, J. Moody, P. Neumayer, B. B. Pollock, J. S. Ross, and S. H. Glenzer, Phy. Rev. Lett., 85 085001 (2007)

6. Laser beam propagation through inertial confinement fusion hohlraum plasmas (invited), D. H. Froula, L. Divol, N. B. Meezan, S. Dixit, P. Neumayer, J. D. Moody, B. B. Pollock, J. S. Ross, L. Suter, and S. H. Glenzer, Phys. Plasmas, 14 055705 (2007)

7. Role of hydrodynamic simulations in laser-plasma interaction predictive capability (invited), N. B. Meezan, R. L. Berger, L. Divol, D. H. Froula, D. E. Hinkel et al., Phys. Plasmas, 14 056304 (2007)

8. Thomson scattering techniques in a laser produced plasma (invited HTPD), D. H. Froula, J. S. Ross, L. Divol, and S. H. Glenzer, Rev. Sci. Instr., 77 10E522 (2006)

9. Implementation of imaging Thomson scattering on the Omega Laser, J. S. Ross, D. H. Froula, A. J. Mackinnon et al., Rev. Sci. Instr., 77 10E520 (2006)

10. 0.351-nm Transmitted Beam Diagnostic at the Omega Laser Facility, D. H. Froula, V. Rekow, C. Sorce, K. Piston, R. Knight, S. Alvarez, R. Griffith, D. Hargrove, J. S. Ross, S. Dixit, B. Pollock, L. Divol, S. H. Glenzer, W. Armstrong, R. Bahr, K. Thorp, and G. Pien, Rev. Sci. Instr., 77, 10E507 (2006)

11. Thomson-scattering measurements of high electron temperature hohlraum plasmas for laser-plasma interaction studies, D. H. Froula, J. S. Ross, L. Divol, N. Meezan, A. J. MacKinnon, R. Wallace, and S. H. Glenzer, Phys. Plasmas 13 (2006)

[1] J. D. Lindl, Phys. Plasmas **2**, 3968 (1995).
[2] B. Remington et al., Rev. Mod. Phys. **78**, 755 (2006).
[3] E. Moses and E. Al., Fussion Sci. Tech. **47**, 314 (2005).
[4] C. Cavailler, Plasma Phys. Control. Fusion **47**, B389 (2005).
[5] R. L. Berger et al., Phys. Plasmas **5**, 4337 (1998).
[6] C. Still et al., Phys. Plasmas **7**, 2023 (2000).
[7] W. L. Kruer, *The Physics of laser plasma interactions* (Addison-Wesley Publishing Company, Inc., 1988).
[8] J. D. Lindl et al., Phys. Plasmas **11**, 339 (2004).
[9] N. B. Meezan et al., Phys. Plasmas **14**, 056304 (2007).
[10] J. M. Soures et al., Laser Particle Beams **11**, 317 (1993).
[11] D. Froula et al., Phys. Plasmas **13**, 052704 (2006).
[12] S. W. Haan, Phys. Plasmas **2**, 2480 (1995).
[13] S. H. Glenzer et al., Phys. Rev. Lett. **82**, 97 (1999).
[14] J. Ross et al., Rev. Sci. Instrum. **77**, 10E520 (2006).
[15] S. H. Glenzer et al., Rev. Sci. Instrum. **70**, 1089 (1999).
[16] A. J. Mackinnon et al., Rev. Sci. Instrum. **75**, 3906 (2004).
[17] D. H. Froula et al., Rev. Sci. Instrum. **77**, 10E507 (2006).
[18] J. Moody et al., Rev. Sci. Instrum. **70**, 677 (1999).
[19] J. Moody et al., Phys. Plasmas **7**, 3388 (2000).
[20] S. Dixit et al., Opt. Lett. **21**, 1715 (1996).
[21] M. M. Marinak et al., Phys. Plasmas **8**, 2275 (2001).
[22] S. H. Glenzer et al., Phys. Plasmas **6**, 2117 (1999).
[23] G. P. Schurtz et al., Phys. Plasmas **7**, 4238 (2000).
[24] B. Macgowan et al., Phys. Plasmas **3**, 2029 (1996).
[25] J. C. Fernandez et al., Phys. Rev. Lett. **81**, 2252 (1998).
[26] B. H. Failor et al., Physical Review E **59**, 6053 (1999).
[27] R. L. Kauffman et al., Phys. Plasmas **5**, 1927 (1998).
[28] D. H. Froula et al., Rev. Sci. Instrum. **77**, 10E522 (2006).
[29] J. Sheffield, *Plasma Scattering of Electromagnetic Radiation* (Academic Press INC., New York, 1975).
[30] D. H. Froula et al., Phys. Plasmas **10**, 1846 (2003).
[31] D. E. Evans, Plasma Physics **12**, 573 (1970).
[32] D. H. Froula et al., Phys. Plasmas **9**, 4709 (2002).
[33] S. H. Glenzer et al., Phys. Rev. Lett. **77**, 1496 (1996).
[34] D. H. Froula et al., Phys. Rev. Lett. **98**, 085001 (2007).
[35] C. Tang, J. Appl. Phys. **37**, 2945 (1966).
[36] D. S. Montgomery and R. P. Johnson, Rev. Sci. Instrum. **71**, 979 (2001).
[37] T. Dewandre et al., Phys. Fluids **24**, 528 (1981).
[38] P. Kaw et al., Phys. Fluids **16**, 1522 (1973).
[39] E. A. Williams, Phys. Plasmas **13**, 056310 (2006).
[40] R. P. Drake, *High-Energy-Density Physics* (Springer Berlin Heidelberg, New York, 2006).
[41] P. Michel and L. Divol, To be submitted to Phys. Plasmas (2007).
[42] E. A. Williams, Tech. Rep. UCRL-LR-105820-98, Lawrence Livermore National Laboratory (1998).
[43] E. Lefebvre et al., Phys. Plasmas **5**, 2701 (1998).
[44] H. A. Rose and D. F. Dubois, Phys. Rev. Lett. **72**, 2883 (1994).
[45] D. S. Montgomery et al., Phys. Rev. Lett. **84**, 678 (2000).
[46] H. Baldis et al., Phys. Rev. Lett. **80**, 1900 (1998).
[47] V. T. Tikhonchuk et al., Phys. Plasmas **3**, 3777 (1996).
[48] K. Tsubakimoto et al., Opt. Commun. **91**, 9 (1992).
[49] D. H. Munro et al., Appl. Opt. **43**, 6639 (2004).
[50] S. H. Glenzer et al., Nature Physics **3**, 716 (2007).
[51] D. S. Montgomery et al., Phys. Plasmas **3**, 1728 (1996).
[52] S. H. Glenzer et al., Phys. Plasmas **8**, 1692 (2001).
[53] J. D. Moody et al., Phys. Rev. Lett. **86**, 2810 (2001).
[54] J. Fuchs et al., Phys. Rev. Lett. **84**, 3089 (2000).
[55] S. Huller et al., Phys. Plasmas **5**, 3794 (1998).
[56] R. Berger et al., Phys. Plasmas **6**, 1043 (1999).